Int. J. Heat Mass Transfer. Vol. 35, No. 2, pp. 295–305, 1992
Printed in Great Britain

0017–9310/92 $5.00+0.00

Heat transfer enhancement in the direct contact melting process

AKIO SAITO, HIKI HONG and OSAMU HIROKANE
Department of Mechanical Engineering, Tokyo Institute of Technology, O-okayama 2-12-1, Meguro-ku, Tokyo 152, Japan

(*Received* 5 *February* 1991 *and in final form* 9 *April* 1991)

Abstract—In direct contact melting, it is clear that one of the factors that affect heat transfer is the size of the heat transfer surface. This indicates that the shorter the path through which the liquid between the heat transfer surface and the solid PCM is rejected outside, the thinner the liquid melt, which decreases the thermal resistance between the source and PCM. In the present work, it was investigated how the heat transfer can be promoted by machining slots on the disk-type heat transfer surface and dividing it into several sector-shaped sections, through theoretical analysis, experiments and numerical analysis. Experiments were performed varying the number of splits and the width of slots under different surface temperatures and pressures. Numerical analysis shows a good agreement with experiments. Also, it was found that the prediction equation yielded by theoretical analysis gives not only a qualitative explanation of the increase of heat flux, but also a quantitative prediction of the heat flux with adequate accuracy. Summarizing these results, the enhancement of heat transfer can apparently be achieved according to the number of splits.

1. INTRODUCTION

IN DIRECT contact melting, shown in Fig. 1, a very thin liquid-filled layer exists between the PCM solid and the heating plate, since the liquid yielded by melting is continuously squeezed out of the layer by force which presses the solid against the plate. In general, heat flux across a thin layer from the heated source to the solid is much higher than that of heat transfer dominated by natural convection, which occurs in two relatively thick spaces between source and solid.

Research on direct contact melting has a short history. Bareiss and Beer [1] studied the behavior of direct contact melting analytically for the case of the melting process of an unfixed solid PCM in a horizontal tube. At the same time, Saito *et al.* investigated the phenomenon of direct contact melting on a horizontal heating plate [2, 3] and on an inner surface of a horizontal cylindrical tube [4] through experimental and numerical analysis. Later on, research to clarify the mechanism of the direct contact melting phenomenon was also conducted by Moallemi *et al.* [5, 6]. Through the investigation of other configurations such as the spherical enclosure by Roy and Sengupta [7] and the inclined circular tube by Sparrow and Myrum [8], it has been confirmed that direct contact melting is characterized by its rapid melting rate compared with natural convection-dominated melting. Sparrow and Geiger [9] compared the effect of fixed and unfixed solids in the same experimental device (a horizontal tube) to show that the rate of melting in the direct contact region is in the range of 88–94% of the overall rate of melting and that the heat transfer rate dominated by direct contact melting is superior to that dominated by natural convection.

In the range of Stefan numbers less than 0.1, it is known that the heat transfer across the liquid layer is mainly dominated by conduction [10]. This indicates that the thinner the liquid layer, the less the thermal resistance between the solid PCM and the heating plate, and the greater the increase in heat flux. Taghavi [11] attempted to reduce the layer thickness using centrifugal force and achieved a greater heat flux. However, in an applicable sense, it is rather difficult to apply such an external force to ordinary types of heat transfer equipment. It is, therefore, more appropriate to survey other factors that affect the enhancement of heat transfer. In the present work, the extent of factors influencing heat transfer in the direct contact melting process is discussed and a possible practical method to accomplish it is proposed, and the effect is examined theoretically, experimentally, and analytically.

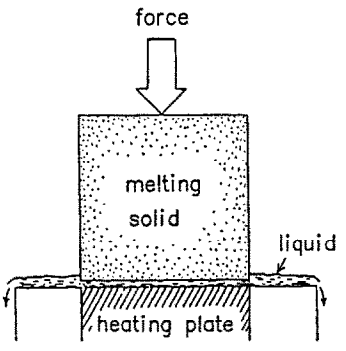

FIG. 1. Schematic diagram of direct contact melting.

NOMENCLATURE

a	thermal diffusivity
A	cross-sectional area of heating plate
c	specific heat
h_m	latent heat of melting
k	thermal conductivity
K	constant, see equation (3)
l	distance from the melt point to the nearest edge through the stream line, see equation (4)
L	average melt travel distance, see equation (4)
n	number of splits of a heating plate
p	static gage pressure in the liquid layer
P	average gage pressure exerted on the solid–liquid interface
P^*	dimensionless pressure, $PR^2/\mu a$
P'	average static gage pressure in the liquid layer, see equation (20)
q	heat flux
q^*	dimensionless heat flux, $qR/(k\Delta T)$
R	radius of heating plate
(r, θ, z)	coordinates, see Fig. 5
Ste	Stefan number, $c\Delta T/h_m$
T	temperature
T_m	melting temperature
T_w	surface temperature of heating plate
ΔT	temperature difference, $T_w - T_m$
u_r	velocity in the r-direction
u_θ	velocity in the θ-direction
v	velocity in the z-direction
V	liquid velocity at solid–liquid interface
X	variable, see equation (3).

Greek symbols

δ	thickness of liquid layer
μ	viscosity of liquid
ρ	density of liquid.

Subscripts

0	heating plate without slot whose cross-section is a circle
n	heating plate with n slots.

Superscript

*	dimensionless quantity.

2. THEORETICAL ANALYSIS

In the case of melting on a horizontal circular plane, the heat flux is determined by several variables. It can, however, be rearranged into three parameters, i.e. dimensionless heat flux q^*, Stefan number Ste and the dimensionless pressure P^*, and the relationship [10] can be formulated as follows:

$$q^* = f(Ste)P^{*0.25}Ste^{-0.25}$$

$$f(Ste) = 0.915 + 0.168Ste. \quad (1)$$

Equation (1) can be rewritten in a dimensional form as follows:

$$q = f(Ste)\left(\frac{P}{\mu a}\right)^{0.25}(k\Delta T)(Ste)^{-0.25}R^{-0.5}. \quad (2)$$

To investigate how each variable pertaining in equation (1) influences the heat flux q, the following relation is used:

$$\frac{\delta q}{q} = K\frac{\delta X}{X} \quad (3)$$

where the constant K can be a measure of the effect of a variable X to the heat flux q, summarized in Table 1. As can be seen in Table 1, the upper three factors, i.e. the temperature difference between the heating plate and melting point ΔT, the thermal conductivity of the liquid k and the radius of the cross-section of solid PCM R, have larger absolute values of K than those of the others below. In the present work, attention is turned to the effect of the solid radius only, while the surface temperature is fixed as it is usually decided by the characteristics of the system.

First, it is explained qualitatively why a smaller radius increases the heat flux under a given surface temperature and pressure exerted on the liquid layer. The decrease of solid radius also reduces the radius of the heating plate, and decreases the average distance through which the melt liquid travels from its own location of melt to the edge of the solid PCM. Here, it is advantageous to define quantitatively the average melt travel distance so as to facilitate the physical description

$$L = \frac{\int_A l\,dA}{\int_A dA}. \quad (4)$$

Table 1. The values of K against the variable X

X	K	
ΔT	$\dfrac{0.686+0.294Ste}{0.915+0.168Ste}$	(0.75–0.768)
k	0.75	
R	−0.5	
P, ρ	0.25	
μ	−0.25	
h_m	$\dfrac{0.229-0.126Ste}{0.915+0.168Ste}$	(0.232–0.25)
c	$\dfrac{0.168Ste}{0.915+0.168Ste}$	(0–0.018)

In this process with decreasing radius, if there is no change in thickness of the liquid layer, the force in the layer becomes unbalanced, since the decrease of the average melt travel distance gives rise to a decrease of pressure drop in the melt flow through the liquid layer with average static pressure decreasing, but the pressure exerted on the solid–liquid interface does not vary. Hence if the liquid layer becomes thinner, it increases the pressure drop, and consequently the static pressure in the liquid layer becomes higher. That, in turn, results in a new force balance on the solid–liquid interface.

The smaller the thickness, the less the thermal resistance across the layer and the greater the heat flux. This can also be deduced by analyzing equation (2). In this equation, if the relation of the heat flux q and the radius R only is considered, it can be rewritten as

$$\frac{q}{q_0} = \left(\frac{R}{R_0}\right)^{-0.5} \tag{5}$$

where subscript 0 denotes a selected reference. This equation indicates that the rate of heat transfer is inversely proportional to the square root of the radius of solid PCM.

For a practical application to thermal storage, instead of decreasing the cross-sectional area of the solid PCM, as it is in fact difficult to make it arbitrarily small due to the restriction of the actual size of the heat storage tank, a split heating plate was devised, as shown in Fig. 2. The heating plate with circular cross-section is characterized by the radial slots with the path underneath, which causes a reduction of flow resistance of the liquid melt, depicted in Fig. 2(b). By this means the decreasing effect of the radius of the solid PCM or the average melt travel distance can be obtained. This, in turn, results in the increase of heat flux with decreasing thermal resistance across the liquid layer. It is evident that in the case of a circle the same physical explanation is permissible by using either the radius R or the average melt travel distance (equal to $R/3$). So, equation (5) can be rewritten using the average melt travel distance L:

$$\frac{q}{q_0} = \left(\frac{L}{L_0}\right)^{-0.5}. \tag{6}$$

On the other hand, in a geometry other than a circle, which has no corresponding radius, it seems to be proper only to utilize the average melt travel distance for a qualitative illustration. However, due to a lack of mathematical strictness, the occurrence of some problems are inevitable in extending its usage in quantitative calculations, i.e. to use the average melt travel distance in equation (6) which was deduced in a circle. Nevertheless, it is still worth using it to investigate the tendency of the increase of heat flux according to the average melt travel distance for a non-circular geometry.

Prior to the application to the sector, it is desirable to attempt a relatively simple geometry such as a rectangle. A rectangle with a short-hand side of $2R$ and a long-hand side of infinity has its analytical solution evaluated under the assumption of a linear temperature gradient across the liquid layer, of which the average melt travel distance is $R/2$. Both the established analytical solution [5] and the approximate solution obtained by the method using equation (6) can be arranged in the form of $q^* = \text{constant} \times P^{*0.25} \times Ste^{-0.25}$, where the constant is 0.783 for the former and 0.741 for the latter. Despite having some restrictions as indicated above, it is surprising that the difference lies only within 5%.

We now turn our attention to the sector of a circle. The approach is exactly the same to that of a rectangle, but we need to introduce some assumptions because of the difficulties in determining the average melt travel distance:

(1) the molten liquid runs out towards the nearest edge from the point where the liquid melts;

(2) the trajectory of the melt flow towards the sides shows a circular arc, as shown in Fig. 3.

From these assumptions, it is determined whether the flow is directed towards the sides or the arc of the sector, that is, if

$$0 \leqslant r \leqslant \frac{R}{\theta+1} \tag{7}$$

then flow is towards the arc, and if

$$\frac{R}{\theta+1} < r \leqslant R \tag{8}$$

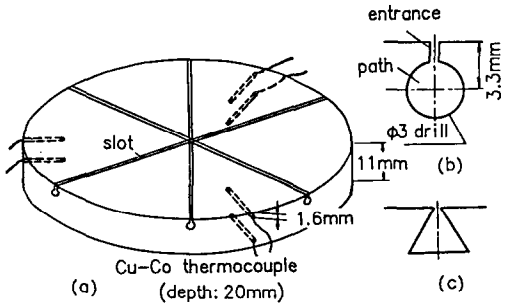

FIG. 2. Heating plate with radial slots and detailed cross-section of slot.

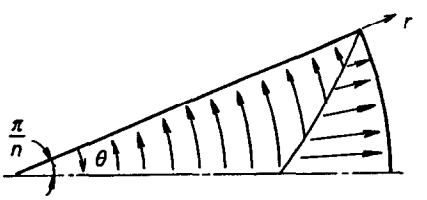

FIG. 3. Schematic diagram of imaginary stream line on the sector of a circle based on equations (7) and (8).

then it is towards the sides, where θ lies between 0 and π/n.

With these in mind, the average melt travel distance L for the sector of a circle can be calculated:

$$L = \left\{\int_0^{R/(\theta+1)}\int_0^{\pi/n} r^2\theta \, d\theta \, dr + \int_{R/(\theta+1)}^{R}\int_0^{\pi/n} (R-r)r \, d\theta \, dr\right\} \Big/ \left(\frac{\pi R^2}{2n}\right) = \frac{\pi R}{3(n+\pi)}. \quad (9)$$

Inserting the obtained value of L into equation (6) using a circular heating plate of radius R as reference point, and rearranging, it is apparent that the sector gives rise to a $(1+n/\pi)^{0.5}$ increase in heat flux compared with that of the circular plate. Therefore, combining this result with equation (1), a prediction equation of heat flux for a sector becomes

$$q_n^* = \left(1+\frac{n}{\pi}\right)^{0.5} q_0^* = \left(1+\frac{n}{\pi}\right)^{0.5} f(Ste)P^{*0.25}\,Ste^{-0.25}. \quad (10)$$

As a reference, in the case of a sector, the same conclusion can be deduced using a hydraulic radius, although it does not always correspond to any geometries.

3. EXPERIMENTAL

3.1. *Experimental apparatus*

The experimental apparatus consisted of a heating plate, injection tubes, weights and others, as shown in Fig. 4. To satisfy the constant surface temperature condition, temperature-regulated water from a constant temperature bath was injected to the lower surface of the heating plate through 50 injection tubes 5 mm in inner diameter. The frame of the device was made of transparent acryl in order to visually observe the inside.

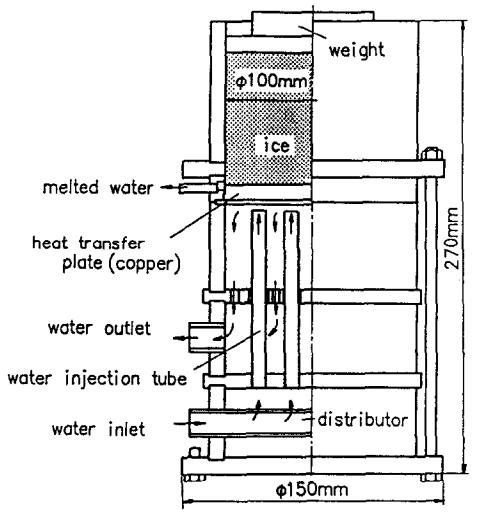

FIG. 4. Experimental apparatus.

The heating plate, explained briefly in Fig. 2, was a copper disk 100 mm in diameter and 11 mm in thickness. On the upper surface of the heating plate, a number of radial slots were machined at equal angular intervals to separate the heating plate into many sector-shaped surfaces. Whether the surface can act as an independent heating source or not is associated with the ability of the slot. The pressure of the sides of the sector needs to be close to that of the circular arc in Fig. 2 so that the liquid melt flows into the sides as well as into the arc. To facilitate the flow of liquid melt along the slots, small holes 3 mm in diameter were drilled beneath the slots (see Fig. 2(b)). This decreases the pressure drop along the path and the pressure distribution of the side can approach the ambient pressure.

The temperature distribution on the surface of the heating plate was measured by copper–constantan thermocouples inserted through small holes drilled at six places, as shown in Fig. 2(a).

To investigate the expected possible effect of the number of splits and the slot width, a number of heating plates were made as illustrated in Table 2.

3.2. *Phase change material*

One of the most important factors in proceeding with the experiment on direct contact melting is the quality of the PCM. If air bubbles or impurities are contained in the PCM specimen, they prevent the melting surface from maintaining a uniform thin liquid layer. Though paraffin and ice are used as the typical PCM specimen, paraffin demands lots of time and effort to become a satisfactory specimen without voids. Hence, it is difficult to select paraffin as a PCM specimen since the present work needs about 150 experiments.

The procedure of preparation of the solid PCM specimen was as follows: first, the commercial ice, which was transparent and included very few voids and impurities, was cut to a suitable size. After putting it into a brass vessel having an inner diameter of 100.5 mm, pure water was poured gently into the empty space between the vessel and the ice. It was then placed in a refrigerator to freeze again until it was completely solidified. Before using it in an experiment, it was laid in cold storage to keep its temperature about 0.5°C below the melting temperature, because its initial tem-

Table 2. Conditions of slot of heating plate used in the experiment

Width of slit (mm)	No. of split					
	4	6	8	12	18	24
0.5	○	○	○	○	○	○
1.0			○	○		
2.0	○		○	○		

Table 3. Experimental conditions for each heating plate: average pressure and surface temperature

Pressure	Mass of weights [g]	133	643	1165	1765
	Pressure range, P^*	4×10^{9}–1×10^{10}	1.1×10^{10}–1.7×10^{10}	1.8×10^{10}–2.4×10^{10}	2.6×10^{10}–3.2×10^{10}
Surface temperature	Temperature range [°C]	0.7 ± 0.2	2.0 ± 0.5	4.5 ± 0.5	8 ± 2
	Range of *Ste*	6×10^{-3}–1.1×10^{-2}	2×10^{-2}–3.2×10^{-2}	5.1×10^{-2}–6.4×10^{-2}	7.6×10^{-2}–1.3×10^{-1}

perature at the refrigerator was too low to use immediately in the experiment.

3.3. *Experimental condition and procedure*

Table 3 presents the experimental conditions for one heating plate, such as the surface temperature of the heating plate and the average pressure exerted on the liquid layer by gravitational force. For one heating plate, 16 experiments were carried out under the conditions of Table 3. The surface temperature can be varied according to the number of splits or the average pressure with the same bath temperature. For this reason, it was almost impossible to set it to a selected temperature, and not actually necessary to do so, since comparison of the behaviors at the same temperature is not the primary purpose of the present work. The temperature of circulating water in a constant temperature bath was controlled by a thermostatically controlled cooler and heater in the bath. After circulating the temperature-regulated water in the apparatus and waiting for thermal equilibrium of the overall experimental device, a block of solid PCM was placed on the horizontal heating plate. On the solid PCM, weights for pressure regulation and vernio-calipus for measuring the timewise variation of solid height were positioned with caution.

Initiation of melting was accompanied by a sudden instability of the experimental system. Measurement was started after about 10% of the solid had melted, which corresponded to recovery of stability. Temperatures at various points were recorded at preselected time intervals. The instantaneous height of the solid was measured using the vernio-calipus and recorded on data sheets in an interval the same as or, if necessary, longer than, that of the temperature.

3.4. *Data reduction*

The surface temperature was obtained by averaging the temperatures adjacent to the upper and lower surfaces, respectively, and extrapolating them. From this value, the Stefan number *Ste* was calculated. The average pressure acting on the liquid layer was evaluated from the resultant forces including the guide plate, weights and the vernio-calipus, as well as the solid PCM. The descent velocity of the solid was determined by differentiation of the instantaneous height of the solid with respect to time.

4. NUMERICAL ANALYSIS

4.1. *Computational model and boundary condition*

First, to facilitate the mathematical formulation, each sector shown in Fig. 2 is considered to lie in the same physical condition and to behave independently. To simplify the computation for the geometry depicted in Fig. 5, the following assumptions were made:

(1) All properties in the liquid layer are constant.

(2) The melting process is quasi-steady: the velocity and temperature fields are invariant with proceeding time.

(3) The flows in the liquid layer show creeping motions [12]: the flow proceeds with very small velocities and the omission of the inertia terms is permissible from the mathematical point of view. The body force is also neglected.

(4) The solid is at its fusion temperature T_m and the surface temperature of the heating plate is uniform at T_w.

(5) The liquid layer has a uniform thickness throughout the heating plate.

(6) The pressures of the sides as well as the arc of the sector are the same as the atmospheric pressure.

Because the thickness of the liquid layer is extremely small compared with the radius of the heating plate, the velocity variations in the r- and θ-directions are much smaller than that in the z-direction. Moreover, the velocity v is much smaller than the velocities u_r and u_θ.

Omitting small terms, the governing equations which express the conservation laws are written in accordance with the above assumptions:

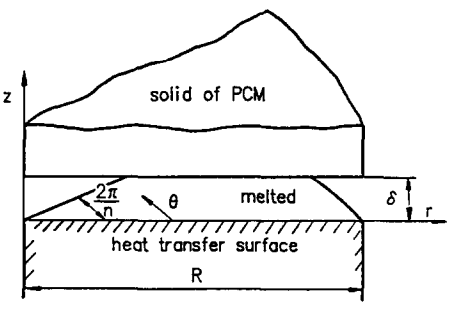

FIG. 5. Geometry and the coordinate system for the direct contact melting region with respect to a sector.

$$\frac{1}{r}\frac{\partial}{\partial r}(ru_r)+\frac{1}{r}\frac{\partial u_\theta}{\partial \theta}+\frac{\partial v}{\partial z}=0 \tag{11}$$

$$\frac{\partial p}{\partial r}=\mu\frac{\partial^2 u_r}{\partial z^2} \tag{12}$$

$$\frac{1}{r}\frac{\partial p}{\partial \theta}=\mu\frac{\partial^2 u_\theta}{\partial z^2} \tag{13}$$

$$u_r\frac{\partial T}{\partial r}+\frac{u_\theta}{r}\frac{\partial T}{\partial \theta}+v\frac{\partial T}{\partial z}=a\frac{\partial^2 T}{\partial z^2}. \tag{14}$$

For the mathematical closure of the problem to be completed, one more equation is needed. That is the force balance on the solid–liquid interface. Neglecting the effect of the inertia of the solid, the equation becomes

$$\int_A p\,\mathrm{d}A=PA. \tag{15}$$

The boundary conditions are:

$$\begin{aligned}
&z=0: \quad T=T_w, \quad u_r=u_\theta=v=0\\
&z=\delta: \quad T=T_m, \quad u_r=u_\theta=0, \quad v=-V\\
&\left(\frac{\partial T}{\partial z}\right)_{z=\delta}=\frac{\rho h_m}{k}(v)_{z=\delta}=-\frac{\rho h_m V}{k}\\
&\theta=0 \quad \text{or} \quad \theta=\frac{2\pi}{n}: \quad p=0\\
&r=R: \quad p=0.
\end{aligned} \tag{16}$$

The procedure of calculation can be simplified by integrating equations (12) and (13) and applying the corresponding boundary conditions. The pressure variation in the z-direction is negligibly small, and $\partial p/\partial z$ is nearly zero. Through the integration by z, therefore, the terms $(\partial p/\partial r)$ and $(\partial p/\partial\theta)$ are treated as constants:

$$u_r=\frac{1}{2\mu}\left(\frac{\partial p}{\partial r}\right)(z-\delta)z \tag{17}$$

$$u_\theta=\frac{1}{2\mu r}\left(\frac{\partial p}{\partial \theta}\right)(z-\delta)z. \tag{18}$$

Substituting equations (17) and (18) into equation (11) and integrating gives

$$v=-\frac{1}{2\mu r}\left(\frac{1}{3}z^3-\frac{\delta}{2}z^2\right)\left\{\frac{\partial}{\partial r}\left(r\frac{\partial p}{\partial r}\right)+\frac{1}{r}\frac{\partial}{\partial\theta}\left(\frac{\partial p}{\partial\theta}\right)\right\}. \tag{19}$$

Inserting the related boundary conditions and rearranging, the pressure equation

$$\frac{\partial}{\partial r}\left(r\frac{\partial p}{\partial r}\right)+\frac{1}{r}\frac{\partial}{\partial\theta}\left(\frac{\partial p}{\partial\theta}\right)=-\frac{12\mu V}{\delta^3}r \tag{20}$$

can be obtained.

In order to solve equation (20), the relation of layer thickness δ and melting velocity V appearing in the right term in the equation is also necessary. It is easily correlated using the result of the literature [5] evaluated based on the postulation of the linear temperature gradient across the liquid layer in a two-dimensional situation on a horizontal plane; that is, the heat transfer is completely dominated by conduction. Despite its seemingly coarse assumption, the comparison with a strict numerical analysis or experiment shows a good agreement within about 3% error in the range of $Ste < 0.1$ [10]. In the present work, to avoid complicated iterative calculations for a more accurate solution, such an assumption is applied. By this means, one more equation to correlate δ and V is introduced as follows:

$$V=\frac{k\Delta T}{\rho h_m \delta}. \tag{21}$$

By substituting equation (21) into equation (20), the complete pressure equation can be formed. Also, the discretization equation which corresponds to this equation was made using the finite-difference method in order to solve it numerically.

4.2. *Calculation procedure*

The optimum number of calculation meshes differs according to the angle of the sector, but the convergence usually appears to be about 15×15, which was used in the actual computation.

The sequence of important operations in the calculation procedure is as follows:

(1) Set the surface temperature T_w and the average pressure P exerted on the liquid layer.
(2) Assume the appropriate layer thickness δ.
(3) Assume the initial pressure distribution p in the liquid layer.
(4) Solve the pressure equation (20).
(5) Compare the new and the old pressure distributions and unless the difference is within the convergence criterion, return to step 3 with the new pressure distribution.
(6) Calculate the average pressure P' in the liquid layer from the converged pressure distribution, and unless the difference between P and P' is within the convergence criterion, return to step 2 with the melt thickness adjusted.
(7) If the converged value of P' is obtained, calculate the melting rate and the heat flux, etc.

5. RESULTS AND DISCUSSION

5.1. *Experimental results*

As a representative result, Fig. 6 shows the relationship between the dimensionless heat flux q^* and the Stefan number Ste, which is the dimensionless counterpart of (T_w-T_m). The figure illustrates the result for split number 8 under dimensionless pressure 1.5×10^{10}, and compares this to the result with no splits. The experiments for the heating plate without slots were also performed to verify the present exper-

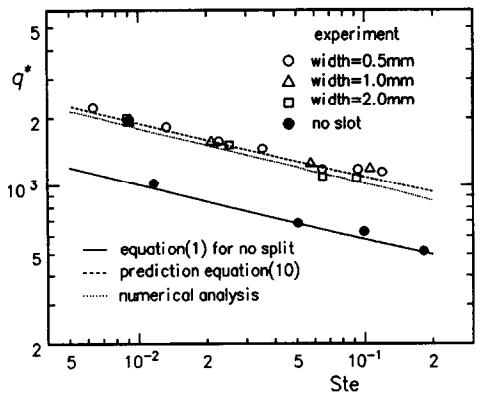

FIG. 6. Dimensionless heat flux vs Stefan number at $P^* = 1.5 \times 10^{10}$ and number of splits = 8, compared with that of no split.

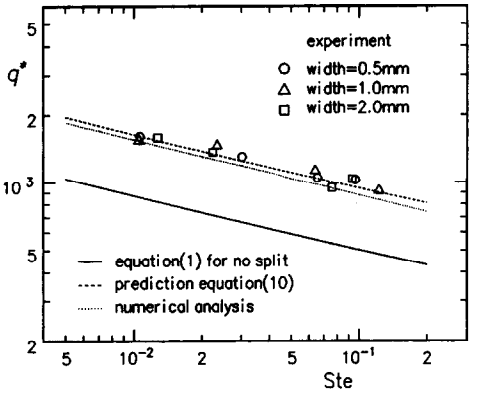

FIG. 7. Dimensionless heat flux vs Stefan number at $P^* = 8.4 \times 10^9$ and number of splits = 8, compared with that of no split.

imental apparatus. It was confirmed to be consistent with the published equation (1) as can be seen in the figure. As witnessed in the figure, the amount of heat flux increases about 1.6 times compared to that of no split, independent of the variation of the surface temperature. The effects of the width of slot, however, did not appear in the experimental range 0.5–2.0 mm, and it is believed that the variation of the slot width in an optimal range does not cause any significant change to the result. The results with respect to numerical and theoretical analysis, which will be explained in detail later, appeared to show good agreement with those of experiments.

It was emphasized that the success of the present split heating plate depends on the ability of the slots, in which the pressure should approach the atmospheric pressure and into which the solid PCM developed should not prevent the liquid melt from flowing. At this stage, though it is difficult to conclude that the slot satisfied such conditions completely, it seems to have some possibilities concerning this ability.

The experiments conducted at a different pressure with the same heating plate showed a similar tendency, as seen in Fig. 7. In spite of the difference in pressure, the heat flux was still around 1.6 times that of no split.

The increasing rate of heat flux does, of course, vary according to the split number, but the pattern of figures was found to be very similar to those of Fig. 6 or Fig. 7. Therefore, to describe the effect of the split number, the data for split numbers 4, 12 and 24, respectively, are summarized in Fig. 8, having the dimensionless pressure 2.2×10^{10} and parametrized by the split number. Figure 9 shows the summarized result of the overall experimental data averaged for each heating plate except for some experiments at which the blockade occurred within the slot, which will be discussed in detail later. The abscissa is set for a split number, while the ordinate is the ratio of heat flux of split heating plate q_n to that of no split q_0. The figure clearly illustrates that the increase of split

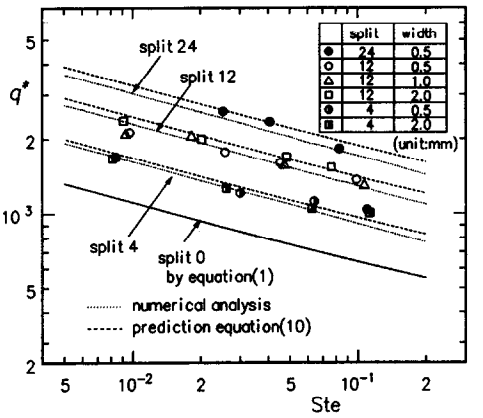

FIG. 8. Effect of split number on dimensionless heat flux at $P^* = 2.2 \times 10^{10}$.

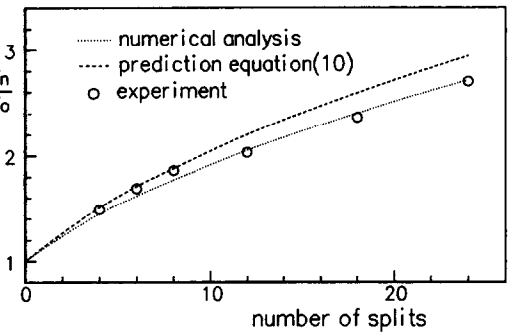

FIG. 9. The ratio of heat flux q_n/q_0 vs number of splits.

number causes a gradual increase of heat flux and, as a consequence, melting rate.

5.2. *Comparison with numerical results*

The results of numerical solutions are presented in Figs. 6–8 along with the experimental data. As shown

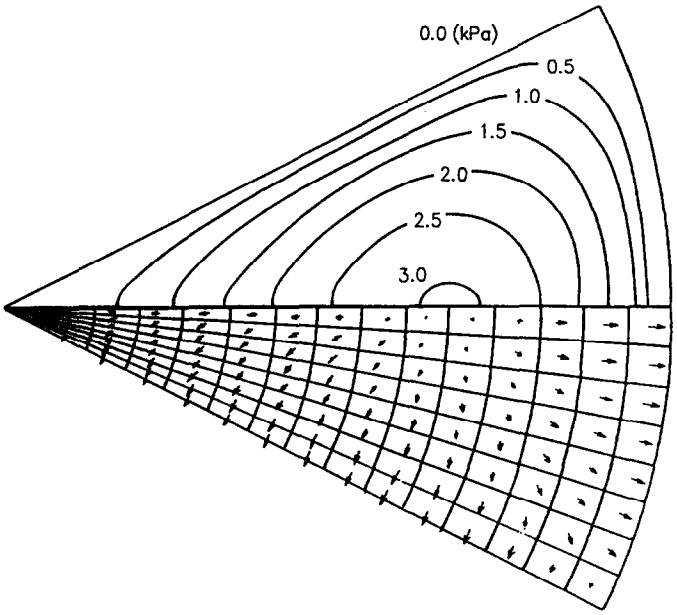

FIG. 10. Velocity vector and pressure distribution in the liquid layer at $P^* = 1.5 \times 10^{10}$, $Ste = 0.05$, and number of splits = 6.

in these figures, the results of numerical solutions lie slightly below those of experiment throughout the range of Stefan number considered. This tendency was observed to be independent of the pressure and the split number. The difference between them, however, tends to increase gradually when the Stefan number increases.

This behavior can be primarily attributed to the assumption of a linear temperature gradient across the liquid gap in numerical solutions. As pointed out earlier, this indicates that the actual heat flux exceeds the evaluated value which includes only the effect of conduction, and the discrepancy becomes larger in the region of higher Stefan number where the convection effect appears more strongly.

The overall observation of the figures, especially Fig. 9, however, illustrates that the experimental and numerical results are in excellent agreement. In addition, a representative example of the distribution of the averaged velocity vector across the liquid layer is displayed in Fig. 10, which is obtained from the results of numerical solutions. Though only half the sector is shown owing to symmetry, it is obvious that the liquid melt runs through the path which is the shortest to either the sides or the circular arc of the sector.

Figure 11 presents the pressure and the velocity distributions along the path beneath the slot, which were evaluated with the postulation of fully developed laminar flow along the path. In order to examine the validity of the aforementioned assumption, the atmospheric pressure along the slot, the numerical solution under the same conditions but with the calculated boundary pressure distribution, as shown in Fig. 11, was obtained as an alternative. The discrepancy of the results between the atmospheric and the alternative turns out to be below 0.3%. The reason for this small difference was due to the maximum pressure on the sector being of the order of thousands of Pascals (Fig. 10), while in the path it was only of the order of tens of Pascals; we thus assume that an atmospheric pressure of 0 Pa does not bring out any serious error.

5.3. *Comparison with approximate prediction*

In Figs. 6–9, it is a little difficult to compare directly the approximate predictions with the experimental data owing to scattering, so they are compared with the numerical solutions. Throughout the entire range

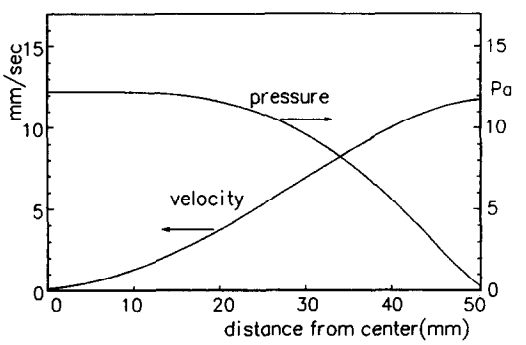

FIG. 11. Velocity and pressure distributions along the path beneath the slot at $P^* = 2.2 \times 10^{10}$, $Ste = 0.05$, and number of splits = 8.

of surface temperatures, exerted pressures and split numbers of the heating plate, the values of the approximate prediction by equation (10) lie slightly above those of the numerical solutions. It was also observed that the discrepancy increases gradually, not only with the increment of the split number but also with the increment of the surface temperature under the same split number. The maximum error was about 7% in the case of split number 12, but if the effect of underestimation of numerical solution stated earlier is considered, the discrepancy does not seem to be so serious.

First, the theoretical analysis was motivated to provide an explanation for the qualitative trend of increasing heat flux in relation to the decreasing size of the heating plate, using the term of average melt travel distance of the corresponding geometry. However, as shown in Figs. 6–9, very good consistency with both the numerical analysis and experiment was obtained.

The imaginary stream line, depicted in Fig. 3, which was set to obtain the average melt travel distance on the sector, seems to be very similar to the velocity vector distribution (Fig. 10) except for the partial region close to the symmetry line.

From these points of view, it may be concluded that the approximate prediction provides quantitative values as well as the qualitative trend.

5.4. *Discussion*

Practical methods to promote the melting rate in the direct contact melting process were examined, and it was concluded that the reduction of cross-section of the solid PCM was one of the most efficient methods. In the present work, instead of decreasing the radius of the solid PCM, an alternative method that can be directly applied to the thermal energy storage system was devised. Radially extended slots were introduced to divide the heating plate into many sectors.

The problem of whether each sector acts completely independently as a heating plate needed to be addressed. However, experimentally determined values only provide a heat flux which shows a relative increase based on the value of no split. Therefore, under the assumption that the sector behaves as an independent heating plate, a numerical analysis was performed. Overall comparison of the experimentally determined results with the numerical solutions illustrated that the effect of the split heating plate devised in this work was beneficial if it acted independently.

Through the experiments, a general phenomenon that the solid PCM protrudes inside the slot, as shown in Fig. 12, was observed visually. For the same slot, the protruding part became further developed in the order depicted in the figure as the pressure was increased or as the surface temperature was lowered. Although the size of the protruding part varied with respect to the width of the slot, the depth in each case was almost even along the radial direction.

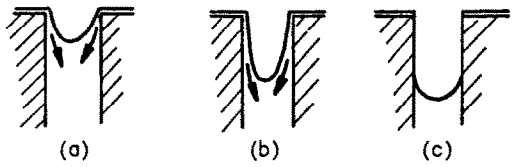

FIG. 12. Growth of protruding solid PCM inside slot (a, b) and predicted value of blockade (c).

The effect of the protruding part for the overall heat flux was investigated in the range of slot width 0.5–2.0 mm. As long as the melting rate decreases gradually with time, it may be believed that there is no significant effect of the protruding part on the melting rate since the heating plate without slots also exhibited such a phenomenon in ref. [10]. For a heating plate with split number higher than 18, some of the experimental results obtained under the condition of comparatively high pressure and low surface temperature showed a slightly different trend, as displayed in Fig. 13. The melting rate, designated as black symbols in the figure, decreased gradually at first and there was then a sudden decrease between 60 and 80 s. On the other hand, the surface temperature of the heating plate also increased at the same time, which indicates a decrease of heat flux through the heating plate. This behavior was primarily considered to be due to the blockade of the slot by the solid PCM, which prevents the liquid melt from flowing into the slots, losing nearly all of its own ability. In order to confirm this phenomenon, the experiment was stopped temporarily when the sudden drop of melting rate was detected until the blocked solid PCM disappeared naturally, and the experiment was then restarted. By this means, it was found that the melting rate and the

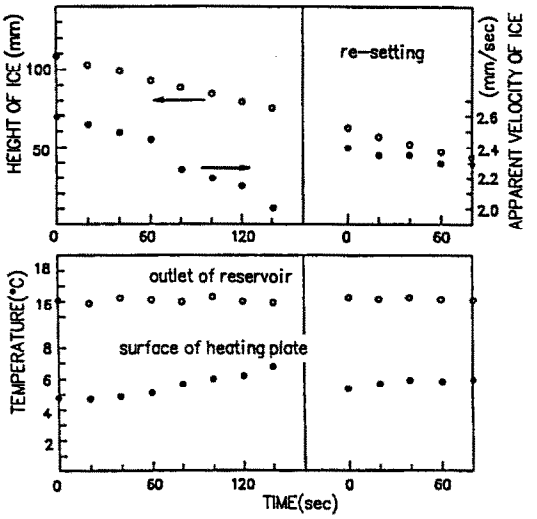

FIG. 13. Timewise variation of melting rate, surface temperature and outlet temperature of bath in experiments where blockade occurred (number of splits = 24, width of slot = 0.5 mm).

surface temperature of the heating plate were restored to their former states, as presented on the right-hand side of Fig. 13.

The possibility of the occurrence of such a phenomenon becomes greater as the pressure exerted on the liquid layer increases, the surface temperature of the heating plate becomes lower, or the split number increases, though it happened only for split numbers greater than 18 in the present work. In order to develop a better understanding of the mechanism of blockade, it may be necessary to note that these three conditions result in a thin liquid layer. The thinner liquid layer between the solid PCM and the heating plate, in turn, gives rise to a narrower gap between the protruding solid PCM and the wall of the slot, which makes the possibility of blockade high. Measuring the thickness of the liquid layer directly is very difficult in a practical sense, but it can be estimated from the heat flux obtained just before blockade occurs, since most of the experimental data are within a region where conduction is dominant ($Ste < 0.1$).

The experimental data in which the blockade has taken place are arranged along with those of no blockade in Fig. 14. The figure presents the surface temperature on the abscissa and the pressure on the ordinate, along with the constant thickness line of the liquid layer. It is clear that many other factors concerning the blockade do exist, such as the kind of PCM and the shape of slot. The shape of slot presented in Fig. 2(c) can be recognized as an example in reducing the blockade in the slot. Hence, further systematical study on the general criteria of blockade will be useful in the usage of split heating plates.

6. CONCLUSIONS

Regarding the melting process dominated by the direct contact melting phenomenon, a method of increasing the heat flux was investigated. It was found that reduction of the cross-sectional area was the most efficient way from a practical point of view. In the present work, a disk-type heating plate on which many slots were machined radially was devised in order to facilitate such an area reduction. Using the theoretical, numerical and experimental approaches, the following conclusions were inferred.

(1) By applying the method presented in this paper, an increasing effect of heat flux was accomplished. It was also found that the increasing rate is not strongly sensitive to the surface temperature of the heating plate, the pressure exerted on the liquid layer and the width of slots in the experimental region. The experimentally determined values approached the numerically evaluated limits, which indicate the values under ideal conditions. Hence, it was concluded that each sector of the split heating plate acted independently.

(2) Numerical solutions agreed reasonably well with the experiments. The existence of a slight difference between them was probably due to the assumption that the heat transfer across the liquid layer is determined only by conduction. Therefore, the adequacy of the mathematical formulation was confirmed.

(3) The average melt travel distance which was introduced in the theoretical analysis was found to be useful in providing not only a qualitative explanation of the increase of heat flux, but also a quantitative prediction with an adequate accuracy.

(4) Some of the experiments performed using heating plates with a split number greater than 18 showed the phenomenon of blockade of slots with solid PCM. The mechanism of blockade was considered and its condition was summarized, though it is restricted in the experimental range of the present work.

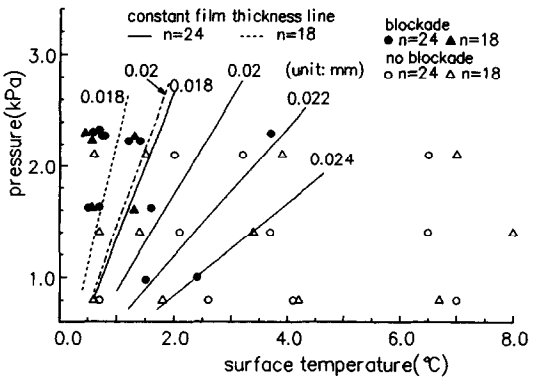

FIG. 14. Experimental conditions when blockade occurred: surface temperature and average pressure with constant thickness line of the liquid layer.

Acknowledgements—The authors express their appreciation to Mr Seiji Okawa, Assistant Professor of TIT, for his contribution in planning the experimental device and in reading the manuscript.

REFERENCES

1. M. Bareiss and H. Beer, An analytical solution of the heat transfer process during melting of an unfixed solid phase change material inside a horizontal tube, *Int. J. Heat Mass Transfer* **27**, 739–745 (1984).
2. A. Saito, Y. Utaka, M. Akiyoshi and K. Katayama, On the contact heat transfer with melting (1st report, experimental study), *Bull. JSME* **28**(240), 1142–1149 (1985) [translated from *Trans. JSME B* **50**(458), 2393–2400 (1984)].
3. A. Saito, Y. Utaka, M. Akiyoshi and K. Katayama, On the contact heat transfer with melting (2nd report, analytical study), *Bull. JSME* **28**(242), 1703–1709 (1985) [translated from *Trans. JSME B* **50**(460), 2977–2984 (1984)].
4. A. Saito, Y. Utaka and Y. Tokihiro, On contact heat transfer with melting (3rd report, the melting on the inner surface of a horizontal cylindrical tube), *JSME Int. J.* **31**(1), Ser. 2, 58–65 (1988) [translated from *Trans. JSME B* **53**(491), 2130–2136 (1984)].
5. M. K. Moallemi, B. W. Webb and R. Viskanta, An experimental and analytical study of close-contact melting, *J. Heat Transfer* **108**, 894–899 (1986).
6. M. K. Moallemi and R. Viskanta, Analysis of close-

contact melting heat transfer, *Int. J. Heat Mass Transfer* **29**, 855–867 (1986).
7. S. K. Roy and S. Sengupta, The melting process within spherical enclosures, *J. Heat Transfer* **109**, 460–462 (1987).
8. E. M. Sparrow and T. A. Myrum, Inclination-induced direct-contact melting in a circular tube, *J. Heat Transfer* **107**, 533–540 (1985).
9. E. M. Sparrow and G. T. Geiger, Melting in a horizontal tube with the solid either constrained or free to fall under gravity, *Int. J. Heat Mass Transfer* **29**, 1007–1019 (1986).
10. A. Saito, Y. Utaka, K. Shonoda and K. Katayama, Basic research on the latent heat thermal energy storage utilizing the contact melting phenomena, *Bull. JSME* **29**(255), 2946–2952 (1986) [translated from *Trans. JSME B* **52**(473), 110–116 (1986)].
11. K. Taghavi, Analysis of direct-contact melting under rotation, *J. Heat Transfer* **112**, 137–143 (1990).
12. H. Schlichting, *Boundary Layer Theory* (7th Edn), pp. 112–113. McGraw-Hill, New York (1979).

ACCROISSEMENT DE TRANSFERT THERMIQUE DANS LE MECANISME DE FUSION PAR CONTACT DIRECT

Résumé—Dans la fusion par contact direct, il est clair que l'un des facteurs qui affecte le transfert thermique est la taille de la surface de transfert thermique. Ceci indique que plus est court le parcours du rejet du liquide entre la surface et le solide PCM, plus mince est le bain liquide qui diminue la résistance thermique entre la source et le PCM. Dans ce travail, on étudie par l'expérimentation et le calcul numérique comment le transfert de chaleur peut être amélioré en réalisant des fentes sur la surface en forme de disque et en la divisant en plusieurs secteurs. Les expériences sont conduites en faisant varier le nombre et la largeur des fentes, la température de la surface et la pression. L'analyse numérique montre un bon accord avec l'expérimentation. On trouve aussi que l'équation obtenue par l'analyse théorique ne donne pas seulement une explication qualitative de l'accroissement du flux thermique, mais aussi une prédiction quantitative avec une bonne précision. En résumé, l'accroissement du transfert thermique peut être réalisé en contrôlant le nombre de fentes.

VERBESSERUNG DES WÄRMEÜBERGANGS BEIM DIREKTKONTAKT-SCHMELZEN

Zusammenfassung—Beim Direktkontakt-Schmelzen liegt es nahe, daß die Größe der wärmeübertragenden Fläche einen entscheidenden Einfluß auf den Wärmetransport ausübt. Dies zeigt, daß je kürzer der Weg ist, durch den Flüssigkeit zwischen wärmeübertragender Fläche und festem PCM abgeschieden wird, desto dünner auch die flüssige Schmelze ist, die den thermischen Widerstand zwischen Quelle und PCM erniedrigt. In der vorliegenden Arbeit wird theoretisch, experimentell und numerisch untersucht, wie der Wärmetransport durch Einarbeiten von Schlitzen auf der tellerförmigen Wärmetauscheroberfläche, die die Fläche in mehrere Sektoren unterteilt, unterstützt werden kann. Die Experimente werden für eine unterschiedliche Anzahl und Breite der Schlitze und für verschiedene Oberflächentemperaturen und Drücke ausgeführt. Die numerische Betrachtung zeigt gute Übereinstimmung mit den Versuchsergebnissen. Es kann auch gezeigt werden, daß die Bestimmungsgleichungen, die man aus den theoretischen Betrachtungen erhält, nicht nur eine qualitative Erklärung für die Zunahme des Wärmestroms ergeben, sondern auch eine quantitative Vorhersage des Wärmestroms mit hinreichender Genauigkeit ermöglichen. Zusammenfassend läßt sich sagen, daß die Verbessergung der Wärmeübertragung anscheinend mit der Anzahl der Schlitze zusammenhängt.

ИНТЕНСИФИКАЦИЯ ТЕПЛОПЕРЕНОСА В ПРОЦЕССЕ КОНТАКТНОГО ПЛАВЛЕНИЯ

Аннотация—Одним из факторов, влияющих на теплоперенос в процессе контактного плавления, является резмер поверхности теплообмена. Это означает, что, чем меньше длина пути, по которому отводится жидкость, содержащаяся между поверхностью теплообмена и твердым материалом в состоянии фазового перехода, тем тоньше слой расплава, благодаря чему уменьшается тепловое сопротивление между источником и материалом. В настоящей работе с помощью теоретического и численного анализа, а также специальных экспериментов исследуется возможность интенсификации теплопереноса посредством нарезки щелей на дискообразную поверхность теплообмена и разделения ее на ряд секторов. В проведенных экспериментах изменялись число щелей и их ширина при различных температурах поверхности и давлениях. Результаты численного анализа хорошо согласуются с экспериментальными данными. Показано также, что выведенное на основе теоретического анализа уравнение не только дает качественное объяснение увеличения плотности теплового потока, но также позволяет определить его количественно с достаточной точностью. Таким образом, интенсификация теплопереноса находится в прямой зависимости от количества щелей.